

## Initial Oxidation of Si(100)-(2 × 1) as an Autocatalytic Reaction

Maki Suemitsu, Yoshiharu Enta, and Yasushi Miyanishi

*Research Institute of Electrical Communication, Tohoku University, 2-1-1 Katahira, Sendai 980, Japan*

Nobuo Miyamoto

*Faculty of Engineering, Tohoku Gakuin University, Tagajo, Miyagi 985, Japan*

(Received 17 November 1998)

Time evolutions of O 2*p* intensity from real-time ultraviolet photoelectron spectroscopy were obtained for the initial oxidation of Si(100)-(2 × 1) surfaces at oxygen pressures  $P = 7.5 \times 10^{-8}$ – $2.8 \times 10^{-6}$  Torr and temperatures  $T = \text{RT} - 720^\circ\text{C}$ . Despite the separation of the growth mode into the Langmuir-Hinshelwood mode in the low- $T$ -high- $P$  region and the 2D-island growth in the high- $T$ -low- $P$  region, they were unifiedly described by a single rate equation for the oxide coverage  $\theta$ , which assumes two types of surface oxygen monomers and the number density of oxide islands that scales with  $\theta(1 - \theta)^2$ . [S0031-9007(99)08678-0]

PACS numbers: 68.45.Da, 82.65.Pa

In response to recent shrinkage of the metal-oxide-semiconductor (MOS) devices and subsequent reduction of the gate-oxide thickness, there has been an increasing demand toward detailed elucidation of initial oxidation at Si(100) surfaces by oxygen. Various studies have been made on this system using photoelectron spectroscopy, scanning electron microscopy, or scanning tunneling microscopy (STM), which yield a common understanding that the oxidation occurs only in the low-temperature-high-pressure regime of the oxidation parameters, while etching results in the high-temperature-low-pressure regime [1,2].

At the boundary between the two regimes, the dynamical behavior of the oxidation may also vary significantly [2–4] and is therefore of great interest both from science and technology viewpoints. Previous studies, however, provide insufficient knowledge in this respect, for they were mostly conducted in the *cook-and-look* mode, where characterization is made intermittently after each short oxidation. This disadvantage is especially critical for Si(100) surfaces, which, unlike (111) surfaces, show no alternation of crystallographically nonequivalent surfaces as the oxide front proceeds into the bulk.

The kinetic change at the oxidation/etching boundary is drastic and can be viewed as a “phase transition” of a two-dimensional gas-liquid system. This conception may have motivated researchers to construct models to describe the oxidations in the high-temperature region based on the surface diffusion and reactions [5,6]. In particular, the single-oxide-species (SOS) and the dual-oxide-species (DOS) model proposed by Engstrom *et al.* [6] seem to cover most of the essentials of the surface processes relevant to oxidation. In these models, one (SOS) or two (DOS) types of oxygen monomers are considered on the Si(100) surface, and the monomers contribute to the Si oxidation via either nucleation or the growth of the oxide clusters. In the DOS model, only the second monomer (monomer-2) contributes to the oxidation, while the first

monomer (monomer-1) desorbs with or without etching. Seiple *et al.* [7] have supported the DOS model by finding a good agreement in the predicted time evolution of the nucleus density with their STM observation.

The aim of this paper is twofold. One is to report our extensive studies on the ultraviolet photoelectron spectroscopy (UPS) time evolutions during dry oxidations of Si(100) surfaces, for temperatures  $T$  from RT to  $720^\circ\text{C}$  and oxygen pressures  $P$  from  $7.5 \times 10^{-8}$  to  $2.8 \times 10^{-6}$  Torr. This was made possible by the development of the real-time photoelectron spectroscopy instrumentation by Takakuwa [2]. As a result, the time evolutions will be classified, from its behavior, into either the low- $T$ -high- $P$  region or the high- $T$ -low- $P$  region. The other objective is to show that, despite the mode separation, all the time evolutions are unifiedly described by a single rate equation for the oxide coverage, containing only two fitting parameters. The rate equation is derived from the DOS model and turns out to be identical with the one for the autocatalytic reaction, an important reaction in the pattern formation chemistry [8].

Experiments were conducted on the beam line BL-3B at the Photon Factory, the High Energy Accelerator Research Organization, with  $h\nu = 23$  eV. Experimental details are identical to those employed in previous works [2–4,9] except for the photon source. The solid lines in Figs. 1(a) and 1(b) show the O 2*p* intensity for (a)  $P = 2\text{--}10 \times 10^{-7}$  Torr at  $T = 640^\circ\text{C}$  and (b)  $T = 580\text{--}640^\circ\text{C}$  at  $P = 2 \times 10^{-7}$  Torr, respectively. The background signal from the Si valence band has been removed by subtraction. Since the proportionality of the O 2*p* intensity with that of the oxide coverage has already been demonstrated [2,9,10], these temporal behaviors correspond to those of the oxide coverage. It is obvious from the figures that the time evolution is of a Langmuir-Hinshelwood type at high pressures or low temperatures, and it becomes sigmoidlike at low pressures or high temperatures. The change is especially drastic

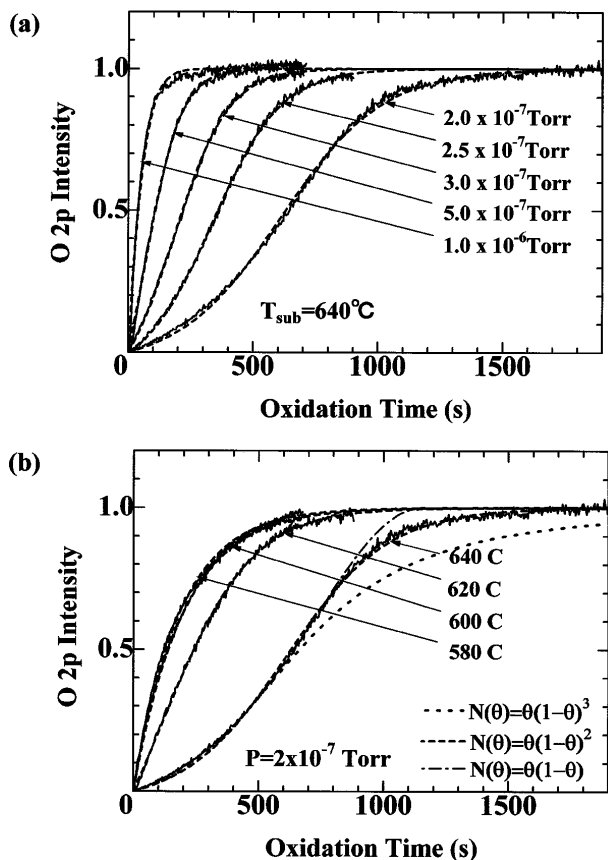


FIG. 1. Time evolutions of O 2p UPS intensity for (a)  $P = 2-10 \times 10^{-7}$  Torr at  $T = 640^\circ\text{C}$  and (b)  $T = 580-640^\circ\text{C}$  at  $P = 2 \times 10^{-7}$  Torr, respectively. The dashed lines are a fitting with Eq. (9), whereas the dotted and the dash-dotted lines in (b) are calculated with the functional forms for  $N(\theta)$  as shown in the figure.

in Fig. 1(b), in which the temperature rise of  $20^\circ\text{C}$  from  $580$  to  $600^\circ\text{C}$  causes essentially no effect, while the same increment from  $620$  to  $640^\circ\text{C}$  causes a significant delay.

To construct a model to describe these behaviors, we start with the DOS model, although most of the following argument is also applicable to the SOS model. The rate equations of the DOS model are given by

$$\frac{d\theta}{dt} = k_a P(1 - \theta) - k_d \theta_1, \quad (1)$$

$$\frac{d\theta_1}{dt} = k_a P(1 - \theta) - k_d \theta_1 - k_c \theta_1 + k_r \theta_2, \quad (2)$$

$$\begin{aligned} \frac{d\theta_2}{dt} = & k_c \theta_1 - k_r \theta_2 - k_n \left( \frac{\theta_2}{1 - \theta_3} \right)^2 (1 - \theta_3) \\ & - k_g \frac{\theta_2}{1 - \theta_3} \sqrt{N \theta_3}, \end{aligned} \quad (3)$$

where  $\theta (= \theta_1 + \theta_2 + \theta_3)$ ,  $\theta_1$ , and  $\theta_2$  denote the surface coverages [monolayers (ML)] of the total oxide, monomer-1 ( $M_1$ ), and monomer-2 ( $M_2$ ), respectively. The coverage of oxide islands is  $\theta_3$  with its number density being  $N$ . The rate coefficients  $k_a$ ,  $k_d$ ,  $k_c$ ,  $k_r$ ,  $k_n$ , and  $k_g$  are to describe adsorption of oxygen, desorption of  $M_1$ ,

conversion of  $M_1$  into  $M_2$ , reconversion of  $M_2$  back into  $M_1$ , nucleation of the oxide island, and growth of the oxide island, respectively, with their activation energy being  $E_\alpha$  ( $\alpha = a, d, c, r, n, \text{ and } g$ ). The monomer-1 is the immediate adsorbate after  $\text{O}_2$  chemisorption, which simply desorbs or etches the surface Si atoms in the form of  $\text{SiO}$ . In addition to desorption,  $M_1$  can be converted to  $M_2$ , which either associates on the surface to form a nucleus or is incorporated into an existing island at its perimeter to contribute its growth [11], but its reconversion into  $M_1$  should also be taken into account. For a specific form of  $M_1$  and  $M_2$ , an isolated oxygen adatom and a bridging oxygen atom may be considered for each [6]. The normalization of  $\theta_2$  with  $1 - \theta_3$  in Eq. (3) represents the fact that the encounter probabilities are proportional, not to the overall coverage, but to the local density of  $M_2$ .

At room temperatures, we can neglect the desorption of  $M_1$  or its conversion into  $M_2$ . The rate equation becomes a conventional Langmuir-Hinshelwood type [3,4],

$$\frac{d\theta}{dt} = k_a P(1 - \theta). \quad (4)$$

The predominance of  $M_1$  in the RT-grown oxides has been evidenced by our recent real-time x-ray photoelectron spectroscopy observation [12], in which  $\text{Si}^{1+}$  is the dominant suboxide species in the oxide. As for the temperature dependence of the adsorption coefficient  $k_a$ , both theory [13] and experiment [14] suggest that it is temperature independent, which explains the temperature-independent time evolutions of the oxide coverage observed below  $550^\circ\text{C}$  [3,4].

As the oxidation temperature increases up to  $550-600^\circ\text{C}$ , the time evolution becomes slightly temperature dependent although it retains the Langmuir-Hinshelwood shape, as shown in Fig. 1(b). This is due to the thermal activation of desorption in this intermediate temperature region, where the oxide growth proceeds via a competition between thermal desorption and conversion into  $M_2$ , a more stable form of the oxide species. The rate equation (1) then becomes

$$\frac{d\theta}{dt} = \frac{k_c}{k_c + k_d} k_a P(1 - \theta), \quad (5)$$

which explains the decreasing initial slope as  $T$  increases in the low-temperature region. This decrease cannot be explained by the SOS model, which forms a reason to favor the DOS model in this study.

As oxidation temperature is raised above  $600^\circ\text{C}$ , the desorption term in Eqs. (2) and (3) becomes significant. As a result, a very rapid saturation of both  $\theta_1$  and  $\theta_2$  is established at  $t \approx \tau_1$ , where  $\tau_1 = (k_a P + k_d + k_c)^{-1} \ll (k_a P)^{-1}$ . The saturated values are of the order of  $\theta_1^0 \approx k_a P / (k_a P + k_d + k_c)$  and  $\theta_2^0 \approx (k_c / k_r) \theta_1^0$ , which are both much less than unity. At  $t \approx \tau_1$ , therefore,  $\theta = \theta_0 = \theta_1^0 + \theta_2^0 \ll 1$  is established. For  $t > \tau_1$ , nucleation of oxide clusters and subsequent two-dimensional island growth using  $M_2$  begins to occur. In this situation, the surface oxide is dominated by the oxide islands and hence

$\theta \approx \theta_3$  holds. The rate equation of the total oxide becomes

$$\frac{d\theta}{dt} = \frac{d\theta_3}{dt} = k_n \left( \frac{\theta_2}{1 - \theta_3} \right)^2 (1 - \theta_3) + k_g \frac{\theta_2}{1 - \theta_3} \sqrt{N\theta_3}. \quad (6)$$

We further introduce a few assumptions to obtain a closed form with respect to  $\theta$ . First we employ  $\theta_2 = P(1 - \theta)(k_c k_a)/(k_d k_r)$  derived from Eqs. (2) and (3) using a quasistatic approximation for  $\theta_1$  and  $\theta_2$ . Second, we introduce a specific  $\theta$  dependence of  $N$  as  $N = N_0\theta(1 - \theta)^2$ . This function has a peak at  $\theta = \frac{1}{3}$  and is zero at both ends of the coverage. This behavior reflects the nucleation-growth-coalescence nature of the island growth in the high-temperature region. While this is not the only function that satisfies the requirements, it gives a best fit to the experiment as discussed later. With these assumptions, the rate equation becomes closed with respect to  $\theta$  as

$$\frac{d\theta}{dt} = K_n P^2 (1 - \theta) + K_g P (1 - \theta) \theta, \quad (7)$$

$$= \frac{1}{\tau_0 \theta_0} (1 - \theta) (\theta_0 + \theta), \quad (8)$$

with  $k_n(k_c k_a/k_d k_r)^2 P^2 = K_n P^2 = (1/\tau_0)$  and  $N_0 k_g(k_c k_a/k_d k_r) = K_g P = (1/\theta_0 \tau_0)$ .

Equation (8) is nothing but a rate equation for the autocatalytic reaction  $A \rightarrow B$  [8]. An autocatalytic reaction is characterized by its rate equation, which is proportional to the concentrations not only of the reactant but of the product:  $k[A][B]$ . In our case of high-temperature oxidations, this corresponds to the fact that the oxide growth proceeds at the perimeter of the islands. Therefore, if we think of Si oxidation as an autocatalytic reaction of  $A = \text{Si}$  and  $B = \text{oxide}$  with  $[A]_0 = 1 \text{ ML}$  and  $[B]_0 = \theta_0$ , we obtain Eq. (8). The finite initial value of  $[B]_0 = \theta_0$  can be reasoned in the previous discussion on  $\theta_0 = \theta_1^0 + \theta_2^0$  that  $\theta_0$  is established immediately after introducing the oxygen gas.

The greatest benefit of employing Eq. (8) is that the equation has an analytical solution,

$$\theta = \theta_0 \frac{1 - e^{-\kappa t/\tau_0}}{\theta_0 + e^{-\kappa t/\tau_0}}, \quad (9)$$

with  $\kappa = (\theta_0 + 1)/\theta_0$ . Although Eq. (8) has been derived for high-temperature oxidations, its functional form covers the low-temperature oxidations as well. In fact, Eq. (9) becomes a Langmuir-Hinshelwood type for  $\theta_0 \gg 1$  and a sigmoid type for  $\theta_0 \ll 1$ . Namely, there arises a possibility that Eq. (9) covers all the time evolutions, from the low- to high-temperature regions. Mathematically,  $\tau_0$  determines the initial slope of  $\theta$ , and  $\theta_0$  defines the critical  $\theta$  at which the burstlike increase of  $\theta$  starts. Physically,  $\tau_0 \theta_0$  gives a measure of the incubation time for the nucleation of oxide clusters, and  $\theta_0$  gives the oxide coverage at which the two-dimensional island growth commences.

With only two parameters, Eq. (9) actually provides excellent fits to the experimental data. The dashed

lines in Figs. 1(a) and 1(b) indicate the best fits by the model calculation. Both experimental and theoretical values are normalized at its saturation value. The ability of the model to reproduce the experimental results is obvious for a wide range of oxidation parameters. The dash-dotted line in Fig. 1(b) is the fit using  $N \propto \theta(1 - \theta)$  and the dotted line is for  $N \propto \theta(1 - \theta)^3$ . While both of the functions show similar good fits for low  $\theta$  values, they show deviations at high coverages. The physical meaning behind these functions is as follows. The functional form  $\theta(1 - \theta)^n$  is derived from a differential equation for the island number  $N$  with respect to  $\theta$ :  $(1/N)(dN/d\theta) = 1/\theta - n/(1 - \theta)$ . Indications of this equation can be given by considering the two extremes of the oxidation process. In the early stage of the oxidation where the first term dominates,  $N$  increases with  $d\theta/(\theta/N)$ . With a knowledge that  $\theta/N$  is the average area of the islands, this represents the oxidation via increase of  $N$  rather than the enlargement of individual islands, which is actually the case [7]. The absence of  $n$  in this discussion explains why the initial behavior of  $\theta(t)$  is so insensitive to the choice of  $n$  in Fig. 1(b). In the final stage of the oxidation, on the other hand,  $N$  decreases with  $-nd\theta/[(1 - \theta)/N]$ , which suggests an oxidation accompanied by the coalescence of islands. The factor  $n$  is correlated with the ratio of the average enriched area of each coalesced island to the average interisland area per island.

Figure 2 shows the pressure dependence of  $\tau_0$ . Equations (4), (5), and (7) indicate that  $\tau_0$  should be inversely proportional to  $P$  in the low-temperature region and should be inversely proportional to  $P^2$  in the high-temperature region. The latter power dependence reflects our choice of the reaction order in the third term in Eq. (3) and is thus not unique; the reaction order may increase with the growth temperature, corresponding to the increase of the critical nucleus size. We have therefore fitted the experimental point for  $T \leq 600 \text{ }^\circ\text{C}$  with  $P^{-1}$  and those for  $T > 600 \text{ }^\circ\text{C}$  with  $P^{-n}$  with  $n$  varied. The assumed  $n = 1$  power dependence for the low-temperature region seems reasonable as evidenced in the good fits. A drastic change in the power dependence from  $n = 1$  to 2.0 is observed between 600 and 620  $^\circ\text{C}$ , which also supports our model. A similar observation of higher-order adsorption kinetics has been reported by Seiple and Pelz [15]. Interestingly enough, a second change was observed between 640 and 660  $^\circ\text{C}$ , from  $n = 2.5$  to 3.7, which suggests an onset of three-body nucleation above 660  $^\circ\text{C}$ .

Figure 3 is an Arrhenius plot of  $1/\tau_0$  that was obtained using the  $\tau_0$  values calculated for  $P = 2 \times 10^{-7}$  from the power laws in Fig. 2. The plots are separated into three regions: the low-temperature region with the activation energy of  $-0.144 \text{ eV}$ , the middle-temperature region with the activation energy of  $-3.91 \text{ eV}$ , and the high-temperature region with the activation energy of  $-8.49 \text{ eV}$ . In accord with the indications from Fig. 2, this demonstrates that the oxidation changes its mode at around 600 and 640  $^\circ\text{C}$ . The small, negative activation energy

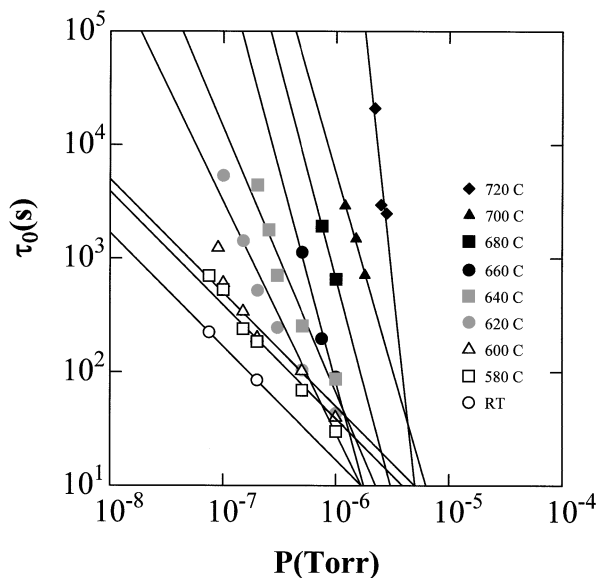


FIG. 2. Oxygen pressure dependence of the fitted parameter  $\tau_0$  for  $RT < T < 720^\circ\text{C}$ . The slope indicates a first-order dependence in the low-temperature regions (open symbols), while the order jumps to 2–2.5 or to 3.5–3.7 in the middle (gray symbols) or the high-temperature (solid symbols) regions, respectively.

( $-0.144\text{ eV}$ ) obtained for the low-temperature region is analyzed using Eq. (5). From the equation, the overall activation energy is given by  $E_c - E_d + E_a \cong E_c - E_d = -0.144\text{ eV}$ . We therefore obtain  $E_c = 3.27\text{ eV}$  for the conversion energy by employing the  $E_d$  value of  $3.41\text{ eV}$  after Engstrom *et al.* [6].

The activation energy of  $-3.91\text{ eV}$  in the middle-temperature region is determined from the temperature dependences of both  $\theta_2$  and the nucleation coefficient  $k_n$  involved in Eq. (7). Since  $\theta_2 = P(1 - \theta)(k_c k_a)/(k_d k_r)$ , the overall activation energy of  $1/\tau_0$  in this middle-

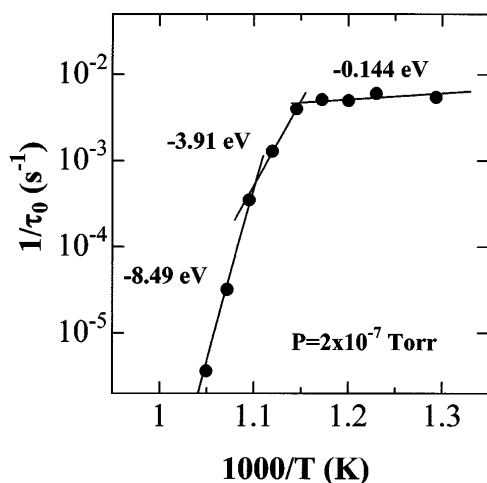


FIG. 3. Arrhenius plot of  $1/\tau_0$  for  $P = 2 \times 10^{-7}\text{ Torr}$ . Fitted values in Fig. 2 were used for the plot.

temperature region is given by  $2(E_c + E_a - E_d - E_r) + E_n \cong 2(-E_d) + E_n = -3.91\text{ eV}$ , provided that  $E_c = E_r$  [7]. Using the value  $E_d = 3.41\text{ eV}$  [6], we obtain  $E_n = 2.91\text{ eV}$ . The value becomes  $3.76\text{ eV}$  if we employ the average power dependence  $-2.25$  instead of  $-2$ . The activation energy of  $-8.49\text{ eV}$  in the high-temperature region can also be analyzed in a similar manner, except that the power dependence now becomes  $-3.5$ . The analysis then yields  $E_n = 3.45\text{ eV}$ , which is in fair agreement with the value obtained from the middle-temperature region.

To conclude, two modes were found to exist in the initial oxidation of  $\text{Si}(100)\text{-}(2 \times 1)$  surfaces: the low- $T$  Langmuir-Hinshelwood growth mode and the high- $T$  two-dimensional island growth mode. They were unified and almost completely described by a single rate equation (the autocatalytic equation) for the oxide coverage  $\theta$ , which was derived from the DOS model together with the number density of islands that scales with  $\theta(1 - \theta)^2$ . With its analytical solution containing only two parameters, the autocatalytic equation may help forthcoming studies obtain deeper insights into the Si oxidation process and ways to control them as well.

- [1] F.W. Smith and G. Ghidhini, *J. Electrochem. Soc.* **129**, 1300 (1982).
- [2] T. Horie, Y. Takakuwa, and N. Miyamoto, *Jpn. J. Appl. Phys.* **33**, 4684 (1994).
- [3] Y. Enta, Y. Takegawa, M. Suemitsu, and N. Miyamoto, *Appl. Surf. Sci.* **100/101**, 449 (1996).
- [4] Y. Takegawa, Y. Enta, M. Suemitsu, N. Miyamoto, and H. Kato, *Jpn. J. Appl. Phys.* **37**, 261 (1998).
- [5] V.D. Borman, E.P. Gusev, Yu. Yu. Lebendinski, and V.I. Troyan, *Phys. Rev. B* **49**, 5415 (1994).
- [6] J.R. Engstrom, D.J. Bonser, M.M. Nelson, and T. Engel, *Surf. Sci.* **256**, 317 (1991).
- [7] J.V. Seiple, C. Ebner, and J.P. Pelz, *Phys. Rev. B* **53**, 15432 (1996).
- [8] P.W. Atkins, in *Physical Chemistry* (Oxford University Press, New York, 1990), 4th ed.
- [9] Y. Enta, Y. Miyanishi, H. Irimachi, M. Niwano, M. Suemitsu, N. Miyamoto, E. Shigemasa, and H. Kato, *J. Vac. Sci. Technol. A* **16**, 1716 (1998).
- [10] Y. Enta, Y. Miyanishi, H. Irimachi, M. Niwano, and M. Suemitsu, *Phys. Rev. B* **57**, 6294 (1998).
- [11] D. Mukesh, W. Morton, C.N. Kenney, and M.B. Cutlip, *Surf. Sci.* **138**, 237 (1984).
- [12] Y. Enta, Y. Miyanishi, H. Irimachi, M. Niwano, M. Suemitsu, N. Miyamoto, E. Shigemasa, and H. Kato (unpublished).
- [13] K. Kato, T. Uda, and K. Terakura, *Phys. Rev. Lett.* **80**, 2000 (1998).
- [14] H. Watanabe, K. Kato, T. Uda, K. Fujita, M. Ichikawa, T. Kawamura, and K. Terakura, *Phys. Rev. Lett.* **80**, 345 (1998).
- [15] J.V. Seiple and J.P. Pelz, *Phys. Rev. Lett.* **73**, 999 (1994).